Lightweight 3D Reconstruction of Urban Buildings From Range Data

Paper ID: 432

Abstract. Laser range scanners are widely used to acquire accurate scene measurements. The massive point clouds they generate, however, present challenges to efficient modeling, visualization, and storage. State-of-the-art techniques for generating 3D models from voluminous range data is well-known to demand large computational and storage requirements. In this paper, attention is directed to the modeling of urban buildings directly from range data. We present an efficient modeling algorithm that exploits *a priori* knowledge that buildings can be modeled using extrusion and taper operations to cross-sectional contours. Inspired by this simplicity, we identify key cross-sectional slices among the point cloud that consist of salient features. Standard image processing algorithms are used to remove noise, fill holes, and vectorize the projected points into contours. Applying extrusion and taper operations to these contours permits us to achieve dramatic geometry compression, making the resulting models suitable for web-based applications such as Google Earth or Microsoft Virtual Earth. This work has applications in architecture, urban design, virtual city touring, and online gaming. We present experimental results on the exterior and interior of urban building datasets to validate the proposed algorithm.

1 Introduction

Automatic 3D modeling of urban buildings is an area of active research with increasing attention drawn from the computer graphics and computer vision communities. Current state-of-the-art algorithms for 3D modeling of urban buildings are computationally expensive and suffer under the weight of large-scale datasets. Despite a recent thrust of activity in 3D modeling and visualization of urban buildings for web-based applications such as Google Earth and Microsoft Virtual Earth, much 3D modeling continues to be manually generated. Applications such as Google SketchUp are popular tools for creating 3D models of urban buildings via an intuitive push-pull modeling interface. This process, however, remains tedious, expensive, and generally produces low-resolution results. This paper seeks to introduce an automatic and efficient algorithm for generating lightweight 3D models of urban buildings directly from point clouds.

The proposed algorithm can generate models across a wide spectrum of resolutions. A particularly useful feature of the algorithm is that even for a low resolution model, the sharpness of the raw data is preserved, thereby outperforming most of the existing approximation techniques. The contribution of this

work is that it combines the benefits of *a priori* knowledge of urban buildings and lightweight 2D image processing techniques to perform 3D modeling of urban buildings directly from point cloud data. This offers the benefit of a cost-effective geometry compression approach for voluminous range data. It can be applied to boost web-based 3D applications, including Google Earth, Microsoft Virtual Earth, virtual city touring and online gaming.

In an attempt to steer clear of tedious and expensive hand-made models, procedural modeling of buildings in [1, 2] has been proposed. By using an effective description language, buildings and streets of a virtual city can be generated automatically. The strength of this approach is that the description language can generate a huge number of buildings and streets quickly and beautifully. This is particular useful for gaming or other computer graphics applications. However, since the parameters used to generate the buildings are randomly generated, the city generated with these buildings and streets is a virtual one. This approach is not useful for attempting to model an *existing* building. In order to do so, one has to manually specify the parameters of the building, which is very cumbersome. Our goal is to automatically infer the parameters of an existing building and therefore reproduce it quickly using the procedural modeling language described above.

There has been a lot of related work on 3D reconstruction in the research community. Essentially, this reconstruction process is the reverse engineering problem of computer graphics [3]. Reverse engineering of range data has been applied in numerous research areas, including computer-aided design (CAD), computer vision, architectural modeling, and medical image processing. In [4], Thompson et al. made use of known manufacturing features to infer the 3D structure of the mechanical parts. Their method benefits from the domain knowledge that most of the mechanical parts consist of predefined structures, such as holes, bosses, and grooves. Our work is partially motivated by this idea since it also incorporates *a priori* knowledge about the construction of urban buildings for further inference. However, their method is based on predefined simple geometry structures and the assumption that the input 3D data has a high signal-to-noise (SNR) ratio. This hinders their approach for those applications with low SNR and incomplete data.

Medical image processing techniques, on the other hand, usually deal with low SNR data. There has been a lot of work on medical 3D image reconstruction. The basic idea behind the vast amount of work conducted in this area is 3D reconstruction from sliced or histologic images using interpolation techniques. Statistical inference is also extensively used to infer the low SNR images. For example, in [5], Sigworth addressed the problem of low SNR images using the maximum-likehood approach. Most of these statistical processes are computationally intensive in order to obtain accurate, high resolution models.

We propose an efficient way to reconstruct 3D models from range data by partitioning the data into thin cross-sectional slabs of volume. For each slab, all range data in that slab is projected onto a 2D cross-sectional image slice. Producing this array of slices permits us to avoid direct computation on 3D data,

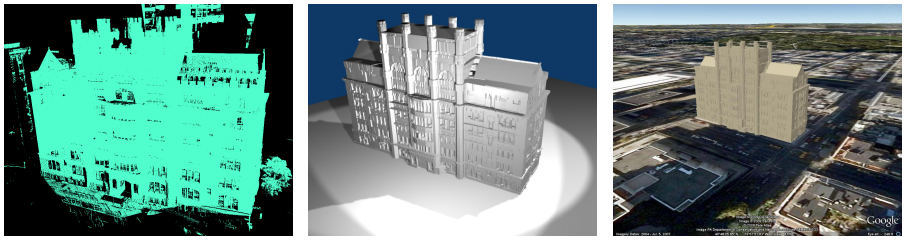

(a) (b) (c)

Fig. 1: (a) A snapshot of the 3D point cloud assembled by registering multiple scans. (b) The lightweight 3D model of the point cloud data reconstructed by our proposed algorithm. (c) The placement of the 3D model on Google Earth.

which is time-consuming and computationally complex. A similarity measure [6] can be used to cluster the sliced images together into *keyslices*. This term is analogous to "keyframes" in computer animation, which denote important moments in the animation sequence from which intermediate results can be derived. Each keyslice is a 2D image which contains the salient cross-sectional structure of a building. We leverage fast 2D image processing techniques on these keyslices to produce lightweight 3D models, consisting of only a few hundred polygons.

2 Preprocessing the Range Data

The input to our system is range data assembled as a 3D point cloud. Our data is obtained from a Leica Cyrax 2500 laser range scanner [7], which works by sweeping an eye-safe laser beam across the scene to collect up to one million 3D depth points per frame. All scene points that lie within 100 meters can be acquired with an accuracy of 5mm in depth. The basic algorithm that we use for registering the voluminous 3D data acquired from multiple scans of buildings has been introduced in [8]. Figure 1(a) shows a snapshot of the registered 3D point cloud, consisting of 14 scans totalling 14 million points.

Due to occlusions and limited vantage points, the point cloud collected by the laser scanner [7] contains noise and missing data. In addition, computing directly on 3D data is time-consuming and computationally complex. To tackle these issues, we define inner and outer bounding boxes for the building to clip away unrelated scene objects. Then, we convert the 3D modeling problem into a set of 2D problems by projecting the 3D data into a series of 2D cross-sectional images. Noise removal, hole filling, and vectorization are all done in this 2D space.

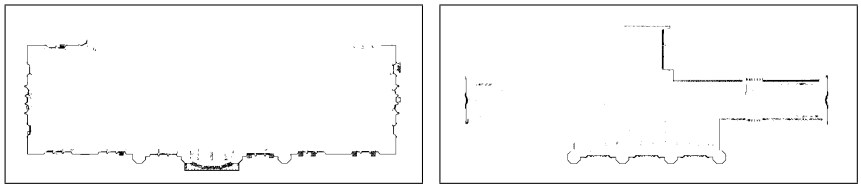

(a) (b)

Fig. 2: The samples of 2D sliced images.

2.1 Extraction of 2D Slices

We consider the point cloud data as a large array of 3D points that can be sliced into horizontal slabs of volume. All 3D points within each slab will be projected onto a horizontal cutting plane, or slice, at the base of the slab. The height of each slab is $\boldsymbol{\delta}$. If that value is held constant, each slice is generated from equal-sized slab intervals. If $\boldsymbol{\delta}$ is allowed to be a dynamic value, then we may choose to allow for large values in parts of the structure that are similar, and low values in regions that contain finer detail. To avoid working on 3D data directly, a relatively small constant value for $\boldsymbol{\delta}$ is chosen to generate 2D cross-sectional image slices.

Without loss of generality, the $y-$axis is used to represent the bottom-up vertical direction. We project the 3D data $\boldsymbol{P}(x, y, z), H_{lo} \leq y < H_{hi}$, in the height range $[H_{lo}, H_{hi})$ onto a 2D image slice. The projection is normalized in the range $[0, W]$, where W is the image width:

$$[\, x^{2D},\ y^{2D}\,]^T = \omega \cdot [\, x_i^{3D} - X_{MIN},\ z_i^{3D} - Z_{MIN}\,]^T \tag{1}$$

Note that $\omega = W/(X_{MAX} - X_{MIN})$, and that the $[X_{MIN}, X_{MAX}]$ and $[Z_{MIN}, Z_{MAX}]$ pairs define the 3D bounding box, which can be obtained through user input and can be used to clip away noise data. Fig. 2(a)-(b) show some examples of the 2D slices, where noise and incomplete data are observed.

2.2 Missing Data Recovery

The slices we extract above are often filled with holes due to occlusion or other visibility issues. Fortunately, most urban buildings have symmetry that we can exploit to fill these holes. Symmetry computation on 3D data [9, 10] is expensive, so we conduct this computation on the 2D image slices. Since the 3D data has been already rectified [11] and projected onto 2D slices, hence only 2D translation is needed to be considered for symmetry computation. Let $P(x, y)$ be a point on the original image I and $P'(x', y')$ be the reflected point of P with respect to a symmetry line L. The symmetry computation equation for L is as follows:

$$L = \arg\min_{x,y} \sum d_{x,y}(P', I) \tag{2}$$

where the $d_{x,y}(P', I)$ is the distance between the self-reflected point P' and its nearest data point in image I. The reflected point P' of the original point P is computed with respect to a line along either the $x-$ or $y-$ axis. Therefore, the symmetry line L is obtained as the line with minimum summation error over the reflected data points.

3 Lightweight 3D Reconstruction

Our 3D reconstruction algorithm is based on *a priori* knowledge that urban buildings can be created through a series of extrusion and taper operations on the salient cross-sections contained in the keyslices. It is therefore critical to identify those salient cross sections upon which the extrusion and taper operations will apply. This will be the key step for successful modeling.

3.1 Extrusion Detection

The 2D image slices of an extruded region are similar to each other. Thus, to detect an extrusion region one only needs to compute the similarity between adjacent slices. The Hausdorff distance is chosen here as the similarity measure. Let $P_r(x_r, y_r)$ be a data point in a reference image and let $P_i(x_i, y_i)$ be a data point in a new observed image I. The Hausdorff distance of image I to reference image I_r is defined as:

$$d_H(I, I_r) = \sum_{i=0}^{N} d_{min}(P_i, I_r) \tag{3}$$

where $d_{min}(P_i, I_r)$ is the minimum distance from data point P_i in image I to the reference image I_r. Alternatively, we can also define the Hausdorff distance, $d_H(I_r, I)$, from reference image I_r to a new observed image I, using the equation 3. These two distances are usually not equal to each other. As a rule of thumb, one can choose $d_{HD} = \text{MAX}\{d_H(I, I_r), d_H(I_r, I)\}$ as the Hausdorff distance. To compute the keyslices, a threshold τ_d is used for the Hausdorff distance d_{HD}. If $d_{HD} < \tau_d$, the two images I and I_r are considered similar to each other. Otherwise, a keyslice image is found and I_r is updated with I, the new keyslice image.

The accuracy of the keyslices detected by using the Hausdorff distance is mainly dependent on the threshold τ_d. Small τ_d leads to more accurate models and will require more time and space to compute and store the result. Therefore, there is a trade-off between model accuracy and time-space efficiency.

3.2 Boundary Vectorization

After the keyslices are detected, N_K keyslices will be identified from a total of N_A image slices. Depending on the threshold τ_d, N_K is usually about one to two orders of magnitude smaller than N_A, e.g., N_K/N_A is 0.06 when $\tau_d =$

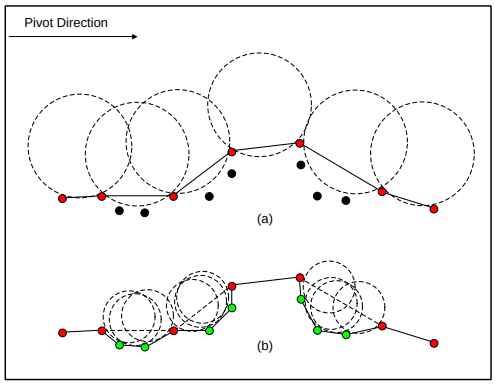

Fig. 3: Ball pivoting: (a) initial pivoting and (b) refinement with smaller radius

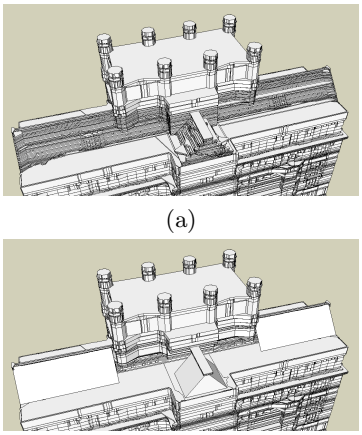

(a)

(b)

Fig. 4: Models of (a) no tapered, (b) with tapered structure

4.0 for the example in Figure 1(a). To generate the 3D model, these keyslice images need to be vectorized to represent the silhouette or boundary of the building. Several raster image vectorization approaches are proposed in [12, 13]. The Douglas-Peucker algorithm attempts to connect all of the existing points to form a polygon. Although the implementation of this approach is very efficient with the improvement described in [14], this method cannot handle the case where spurious interior points are present, which contributes to outlier data. To tackle this issue, we adapted the ball-pivoting algorithm (BPA) [15] from its original use on 3D point cloud data to use on 2D keyslice images where it produces vectorized boundaries. The key parameter for the BPA algorithm to work successfully is to find the right size of the ball for pivoting. We propose a coarse-to-fine adaptive BPA algorithm, described below, to solve this problem.

Due to the gap between data points, a relatively large radius r is chosen as a coarse step to ensure that the ball will travel across all boundary data before turning back or reaching any existing boundary points. Figure 3(a) shows an initial ball-pivoting process on 2D data points. The output of the initial BPA $\boldsymbol{\Phi}$ contains an ordered list of the boundary data points $\boldsymbol{P}$ and their corresponding directions $\overrightarrow{\boldsymbol{R}}$ in which the circle C starts pivoting. The iterative BPA refinement process is applied on $\boldsymbol{\Phi}$ to get more accurate results with a smaller radius $r' = r/2$ as shown in Figure 3(b). The length of each line segment formed by adjacent points is checked, $\ell = \overline{P_0 P_1}$, in $\boldsymbol{\Phi}$. If this line is long enough, the BPA is applied between the two adjacent points. When the ball reaches the second point, a new list of ordered boundary points, $\boldsymbol{\Phi'}$, is inserted into $\boldsymbol{\Phi}$ between P_0 and P_1. This process continues until it finishes checking every adjacent point in $\boldsymbol{\Phi}$. The refinement stops when r' falls below threshold τ_r.

3.3 Tapered Structure Detection

After the keyslices are detected and vectorized, the silhouettes of $N_K = \{I_i, i = 0, ..., K\}$ keyslices can be used to represent the whole building based on the extrusion operation. That is, the space between each pair of keyslices, say I_i and I_j, can be interpolated by the lower keyslice, e.g., I_i in this case. This is valid due to the similarity between the intermediate images and the keyslice I_i. By modeling a building using this series of keyslices N_K, we can largely reduce the space needed to store urban buildings. This helps make possible 3D web-based applications such as 3D city navigation.

In addition to the extrusion operation, we can further improve the model and reduce the model size by observing that part of the keyslice images belong to the same tapered structure. This is demonstrated in Figure 4. Figure 4(a) shows the roof structure of the reconstructed model based on a keyslice image extrusion operation with almost half of the keyslice images dedicated to the roof structure. After applying the tapered structure inference, Figure 4(b) shows the improvement of the modeling. As we can see, the roof in Figure 4(b) is much smoother than that in Figure 4(a). In addition, the keyslices needed to represent the building, and its associated storage, are reduced almost in half.

The difficulty of inferring tapered structure lays on the complication of the building structure itself. Let's assume that the height range for roof structure is $H_R = [H_{lo}, H_{hi}]$. If this is the only existing structure between H_R, it is simple and straight-forward to detect and infer this part. However, for some complicated structures, such as a mixed layout of tapered and extruded structures, some special treatment is needed to obtain the desired results. Our approach is based on the divide and conquer strategy: the whole structure $\boldsymbol{U}$ is segmented into independent sub-structures, $U_0, U_1, \ldots, U_N$. For any sub-structure U_i, it contains only a unique structure, either a tapered or an extruded one. Once each unit U_i is inferred, the whole structure can be modeled by an union operation of these sub-structures, i.e., $\boldsymbol{U} = \bigcup U_i \{i = 1, \ldots, N\}$. Before segmentation, the potential height ranges H_R containing the tapered structures should be computed. This can be done by checking the frequency of the keyslice images. The structure containing tapered sub-structures will show a high and even distributed keyslice images. This is a very useful clue for H_R detection.

Once the potential height ranges H_R is obtained, the next step is to segment the whole structure $\boldsymbol{U}$ between H_R into sub-structures, $U_i,\ i = 0, \ldots, N$. This is again done by similarity measurement of sliced images from orthogonal directions. As before, the 3D data points following inside the range of H_R are projected along both left-right (X axis) and face-inside (Z axis) directions. Then the keyslice detection is carried out based on Hausdorff distance similarity measurement for both directions. These keyslices will segment the structure in H_R into sub units of $U_0, U_1, \ldots, U_N$.

For each sub unit U_i, we have to know whether it represents an extruded or a tapered structure. The method is to check in the keyslice image I_k of U_i whether there exists a pattern where two lines intersect with some appropriate angle. If such a pattern exists in I_k, the unit U_i is marked as a tapered sub-structure.

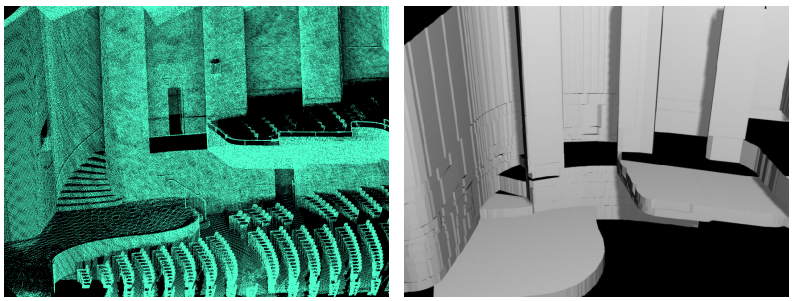

(a) (b)

Fig. 5: The model of an interior scanning. (a) The snapshot of the interior scanning point cloud data. (b) the model reconstructed from the interior scanning.

Otherwise, U_i is marked as an extruded sub-structure. If U_i is an extruded unit, its silhouette from the $y-$ axis is vectorized and is ready for the union operation to obtain $\boldsymbol{U}$. On the other hand, if U_i is a tapered unit, the bottom and top position have to be computed so that it can be reconstructed. To do this, all line segments $\boldsymbol{L}$ in U_i are computed using the Hough Transform and the intersection point P_0 of $\boldsymbol{L}$ indicates the top position of the tapered unit. The other end points P_i of $\boldsymbol{L}$ are also computed to infer the bottom shape and position.

4 Experimental Results and Conclusion

The results of the extrusion and tapered structures computation, together with raster image vectorization, are stored in the 2D image coordinate system. To generate the final 3D model, these data need to be transformed back into the 3D world coordinate system. Let $P(x, y)$ be a point in the 2D image coordinate system, and let $P'(x, y, z)$ be the 3D world coordinate of P, where y is the depth coordinate. For all points in the same boundary layer or silhouette, the points lay in the same plane and hence have the same value of y. The equation for transforming P back to P' is a reverse transformation of $\boldsymbol{T_0}$ in the equation 1:

$$[\, x^{3D},\, y^{3D},\, z^{3D}\,]^T = [\, \eta \cdot x^{2D} + X_{MIN},\, \zeta + Y_{MIN},\, \eta \cdot z^{2D} + Z_{MIN}\,]^T \qquad (4)$$

where $\eta = 1/\omega$ and $\zeta = \kappa \cdot \delta$. Here, κ is the index of the 2D slice and δ is the height of a slab described in the Section 2.1. Figure 1(b) shows an exterior 3D model generated by the above transformation. In addition to the exterior model, we have also applied the approach on the range data of an interior scanning. The snapshot of this interior scan is shown in Figure 5(a) and its reconstructed 3D model is shown in Figure 5(b). This model is primarily reconstructed using the extrusion unit, and the chairs and some fine details are ignored. However, the main structures of the interior are captured and the chairs can be added to the model through texture mapping. Please note that the model generated in Figure

Table 1: The error measurement with respected to Hausdorff distance threshold τ_d. The BPA radius threshold $\tau_r = 4$

τ_d(pixel)	Error (mm)	# of faces	Size (KB)
64	0.658	1471	15
32	0.294	3284	32
16	0.141	8574	86
8	0.131	13955	137
4	0.094	27214	261
2	0.088	31331	335

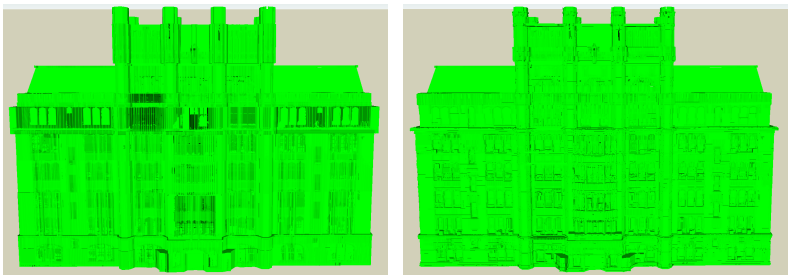

(a) (b)

Fig. 6: The deviation mapping of the 3D point cloud. (a) the result with $\tau_r = 4$ and $\tau_d = 32$. (b) the result with $\tau_r = 1$ and $\tau_d = 4$.

5(b) is of low resolution and some details may lost, which can be captured by using a smaller threshold τ_d to obtain higher resolution models.

To measure the error of a reconstructed 3D model, we first transform it to the 3D point cloud coordinate system. The error is measured as the distance from the sampled 3D points to their closest model planes, which is computed using the following formula:

$$E = \frac{1}{|X|} \sum_{x \in X} d^2(x, M) \tag{5}$$

where X is the set of 3D point cloud data. The distance $d(x, M) = \min_{p \in M} \|x - p\|$ is the minimum Euclidean distance from a 3D point x to its closest face p of M. To visualize the error between real 3D data and the inferred model, we generated the deviation mapping images which are depicted in Figure 6. Basically, for each face p of M, a corresponding texture image is computed. The intensity of each pixel in the texture image is determined by the error of the corresponding 3D points computed by Equation 5. The accuracy of the reconstructed model is mainly controlled by the threshold of Hausdorff distance τ_d and BPA refinement radius τ_r. τ_d determines the accuracy of the keyslice detection and τ_r determines

the accuracy of the boundary vectorization. Table 1 lists the relationship among the τ_d, errors, number of faces and model size. The unit for τ_d is in pixels and for errors is in millimeters. The size for original 3D building point cloud is more than 700 MB. From the table, one can see that even for the most accurate model, the size is dramatically reduced compared with the original 3D point cloud data, which is desired for web-based applications (Fig. 1c).

In conclusion, we presented a lightweight 3D modeling of urban buildings from range data. Our work is based on the observation that buildings can be viewed as the combination of two basic components, the extrusion and the tapering components. The efficient and economical techniques proposed here are used to infer the extruded and tapered unit, and then reconstruct the 3D model via vectorization. The experimental results on both exterior and interior urban building datasets are presented to validate the proposed approach.

References

1. Mueller, P., Wonka, P., Haegler, S., Ulmer, A., Gool, L.V.: Procedural modeling of buildings. ACM Transactions on Graphics (TOG) (2006) 614–623
2. Wonka, P., Wimmer, M., Sillion, F., Ribarsky, W.: Instant architecture. ACM SIGGRAPH (2003) 669–677
3. Fisher, R.B.: Applying knowledge to reverse engineering problems. Computer-Aided Design **36** (2004) 501–510
4. Thompson, W., Owen, J., Germain, H.J., Stark, S.R., Henderson, T.C.: Feature-based reverse engineering of mechanical parts. IEEE Transactions on Robotics and Automation **15** (1999)
5. Sigworth, F.J.: A maximum-likelihood approach to single-particle image refinement. Journal of Structual Biology (1998) 328–339
6. Brown, L.: A survey of image registration techniques. ACM Computing Surveys **24** (1992) 326–376
7. Geosystems, L.: http://hds.leica-geosystems.com/
8.
9. Podolak, J., Shilane, P., Golovinskiy, A., Rusinkiewicz, S., Funkhouser, T.: A planar-reflective symmetry transform for 3d shapes. Proceedings of ACM SIGGRAPH (2006) 549–559
10. Zabrodsky, H., Peleg, S., , Avnir, D.: Symmetry as a continuous feature. IEEE Pattern Analysis and Machine Intelligence **17** (1995)
11.
12. Aronov, B., Asano, T., Katoh, N., Mehlhorn, K., , Tokuyama, T.: Polyline fitting of planar points under min-sum criteria. International Journal of Computational Geometry and Applications **16** (2006) 97–116
13. Douglas, D., Peucker, T.: Algorithms for the reduction of the number of points required for represent a digitzed line or its caricature. Canadian Cartographer **10** (1973) 112–122
14. Hershberge, J., Snoeyink, J.: Speeding up the douglas-peucker line-simplification algorithm. Proceedings of 5th International Symposium Spatial Data Handling (1992) 134–143
15. Bernardini, F., Mittlelman, J., Rushmeir, H., Silva, C.: The ball-pivoting algorithm for surface reconstruction. IEEE Transaction on Visualization and Computer Graphics **5** (1999) 349–359